INDIAN JOURNAL OF SCIENCE AND TECHNOLOGY

RESEARCH ARTICLE

Optimal Unified Triple-Phase-Shift Control Technique for Dual Active Bridge Converter

Pallavi Chaturvedi[1]*, **Mohmmed Rizwan Ansari**[1], **Dheeraj Kumar Palwalia**[1]

1 Department of Electrical Engineering, Rajasthan Technical University, Kota, 324010, Rajasthan, India

OPEN ACCESS

Received: 18-02-2023

Accepted: 17-05-2023

Published: 07-06-2023

Citation: Chaturvedi P, Rizwan Ansari M, Kumar Palwalia D (2023) Optimal Unified Triple-Phase-Shift Control Technique for Dual Active Bridge Converter. Indian Journal of Science and Technology 16(22): 1635-1644. https://doi.org/10.17485/IJST/v16i22.329

* **Corresponding author**.

pallavichat9@gmail.com

Funding: None

Competing Interests: None

Published By Indian Society for Education and Environment (iSee)

ISSN
Print: 0974-6846
Electronic: 0974-5645

Abstract

Objectives: The variable output voltage from the wind energy conversion system is effectively regulated through the Solid-State Transformer (SST) using Dual Active Bridge (DAB) converter employing a Triple phase shift (TPS) control technique. **Methods:** A wind energy based system integrated with SST employing a DAB converter is proposed. The system comprises of Permanent Magnet Synchronous Generator (PMSG) based Wind Energy System (WES), SST, and resistive load. The SST provides an easy interface between the load and the WES.MATLAB Simulink-based analysis is done to compare the various control techniques used for DAB dc-dc converter. **Findings:** The DAB converter provides several benefits including its ability to provide bi-directional power flow, making it suitable for use in applications where power can flow in either direction, such as renewable energy systems. The Single-Phase Shift (SPS) is among the majorly adopted control strategies for DAB converters however it performs unsatisfactorily with varying load conditions. In this paper, a Triple-Phase Shift (TPS) control strategy has been reported. A detailed mathematical analysis along with MATLAB Simulink based results suggest that this control technique reduces current stress on semiconductor switches by reducing peak inductor current by almost 23% and 9% as compared to conventional phase shift modulation technique, therefore, improving the efficiency of the converter**. Novelty:** The phase shift ratio used in the TPS control technique for the DAB converter is modified by incorporating a virtual power component that enhances the dynamic response of the output voltage.

Keywords: Wind Energy System (WES); Solid-State Transformer (SST); Dual Active Bridge Converter (DAB); Triple-Phase Shift (TPS); Single Phase Shift (SPS)

1 Introduction

In today's world, traditional thermal power plants are unable to meet consumer demand through grid utility. Renewable energy resources (RES) such as solar and wind energy have received a lot of attention owing to their reliance on natural phenomena. The global cumulative wind power is expected to reach 2000GW by the year 2030, which is an increment at a rate of 17-19%. Therefore, it would play an important role in supplying

increasing energy demand. The power obtained from wind is variable, and to operate at high efficiency, it requires variable speed control.

The availability of permanent magnet material and newer advancements in power converter technology have attracted wind turbine manufacturers' attention toward direct-drive permanent magnet synchronous generators (D-PMSGs) [1]. PMSGs offer additional advantages, such as improved power factor, no excitation, gearbox elimination, and high efficiency [2]. Additionally, a full-scale back-to-back converter between the PMSG and the load or utility grid in a PMSG-based wind energy system provides complete decoupling of generator-side dynamics and supports grid-side functionalities. A step-up transformer is required to interface the generated low voltage and distribution or transmission system to boost the voltage level [3]. Solid state transformer (SST) is essentially a power electronics device used for applications involving high voltage and power like locomotives and tractions. It utilizes the isolated AC to AC conversion technique of a high-frequency transformer [4].

Solid state transformers are capable of efficiently converting and regulating AC power, making them a suitable option for connecting the AC output of a wind energy conversion system (WES) to a distribution or transmission system. However, in the event of a fault in an islanded mode-operated WES, the SST functions as an isolator between the WES and the connected load. The SST offers superior characteristics and is a feasible substitute for a conventional 50Hz transformer [5]. It has many advantages over conventional transformers, such as reduced weight and size, non-requirement for an input/output filter, no voltage swag or swell, and current limiting capability, among others. The SST has multiple applications, including aerospace applications, DC microgrids, WES, and more.

Numerous power converter topologies have been proposed for solid-state transformers (SSTs) [6,7]. The three-stage SST, which comprises a rectifier, a DAB converter, and an inverter (as depicted in Figure 1), is an optimal choice as it offers greater controllability and encompasses all SST operations. DAB converters are employed because of their simple design along with the advantage of bidirectional power flow and zero-voltage switching (ZVS) operation. For such topologies, there are primarily two types of control methods; traditional pulse-width modulation (TPM) control [8], and phase-shift control [9]. The traditional pulse width modulation control technique is basic and easy to implement on hardware, however, its dynamic performance is poor, and the output voltage is always less than the input voltage.

.

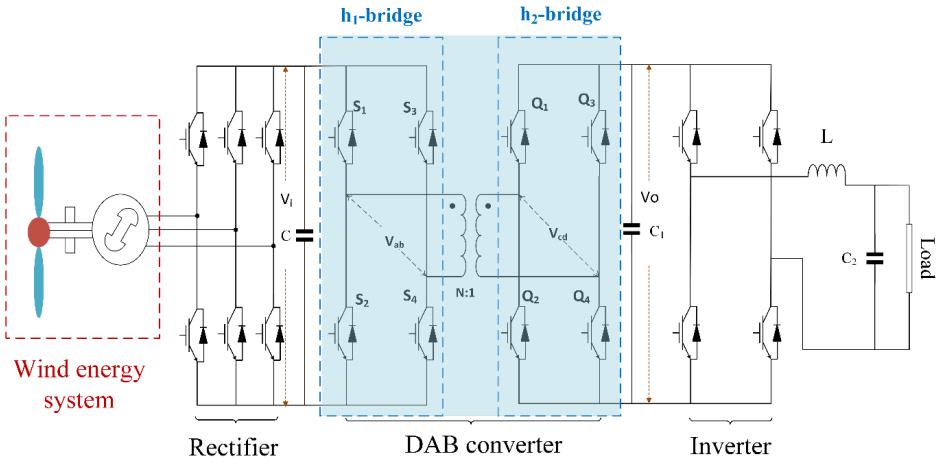

Fig 1. Structural Overview of three stage SST connected with WES

In the SPS control technique, the phase difference between the primary and secondary side of the high-frequency transformer (HFT) is denoted by D1 as shown in Figure 2. The AC voltage equivalent to h1 and h2 bridge is represented by V_{ab} and V_{cd} respectively, with a switching period of T_{sw}.When the voltages on the primary and secondary sides of the HFT are identical, the SPS control technique performs better. However, when voltage transformation ratio k = Input voltage(Vi)/{N* Output voltage (V_o)}is far away from 1 (where N is the turn ratio of the HFT), the SPS approach produces high circulating current, high current stress, and a narrow ZVS band which lowers the efficiency of DAB converter [9,10]. In order to increase efficiency and reduce the current stress of the DAB converter, a dual-phase shift control technique has been discussed [11]. As shown in Figure 3, an additional inner phase-shift ratio D_1 is applied to both sides of HFT. This D_1 is given to both sides of the primary h_1 bridge and the secondary h_2 bridge and the D_2 phase shift is given between two h-bridges. The DPS technique has two conditions based on the relation between D_2 and D_1: $0 \leq D_1 \leq 1$, $0 \leq D_1 \leq D_2 \leq 1$, as illustrated in Figure 3 (a), and $0 \leq D_2 \leq 1$, $0 \leq D_2 \leq$

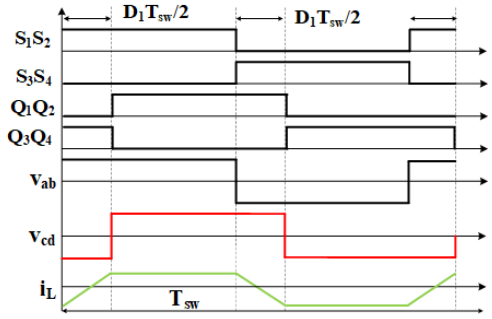

Fig 2. The waveform of SPS control technique

$D_1 \leq 1$, as shown in Figure 3 (b). The advantage of DPS control over SPS control is that it reduces current stress, increases ZVS range, and improves efficiency. DPS control provides better efficiency in buck operation or for transformation ratio (k) < 1 but it performs poorly in boost operation or for (k) > 1.

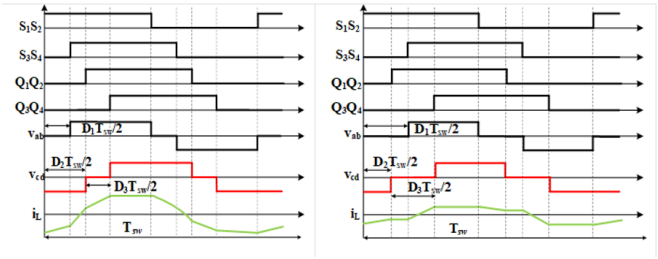

Fig 3. Waveform of DPS control technique (a). $0 \leq D_1 \leq D_2 \leq 1$, (b). $0 \leq D_2 \leq D_1 \leq 1$

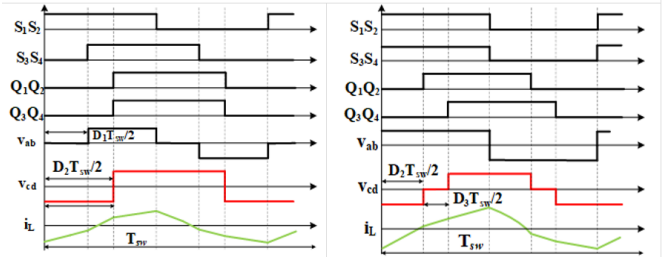

Fig 4. The waveform of the EPS control technique (a). D_1 inner phase shift at h_1-bridge, (b). D_3 inner phase shift at h_2-bridge

To enhance the efficiency of boost operation, the EPS control technique was introduced in [12], which is shown in Figure 4. In this control technique, two-phase shifts are utilized. This technique employs two phase shifts: the inner phase shift ratio (D_1) and the outer phase shift ratio (D_2). The initial phase shift, D_1, reduces circulating power and expands the zero-voltage operating range, while the outer phase shift, D_2, controls both the magnitude and direction of power flow. The EPS control method has two variations based on the position of the inner phase-shift ratio (D_1). It can either be applied to the primary h_1 bridge of HFT, as depicted in Figure 4 (a), or to the secondary h_2 bridge of HFT, as shown in Figure 4 (b). Additionally, the TPS control technique is another phase shift control option that outperforms all other phase shift control methods in terms of performance and efficiency.

2 Methodology

2.1 Triple Phase Shift (TPS) Technique

The triple-phase-shift control technique was proposed in [13], wherein different inner phase-shift ratios D_1 and D_3 are provided in the primary bridge and secondary bridge of HFT, respectively. Phase-shift-ratio D_2 is given in between both h-bridges h_1 and h_2. The TPS control technique can achieve minimum current stress, low switching, and conduction losses, low power loss, and maximum ZVS range with the use of three phase-shift ratios, namely D_1, D_2, and D_3 [14,15]. The proposed topology is represented in Figure 5 (a), where D_1 and D_3 are inner phase shift ratios and D_2 is the phase-shift ratio between h-bridges. Its equivalent circuit is illustrated in Figure 5 (b), where v_{ab} and v_{cd}' are the equivalent AC voltage of two h-bridges referred to as V_1 side. v_{cd}' is calculated as Nv_{cd}, L represents the total equivalent leakage inductance referred to as the primary side of HFT and $V_L = v_{cab} - v_{cd}'$. The value of D_1 and D_2 can vary between 0 to 1 and D_3 can vary between 0 to 2.

The TPS control technique has six different modes, with the output AC voltage waveform of h_1 and h_2 bridges shown in Figure 6 for each mode. In modes d to f, when D_3 is greater than 1, the DAB converter draws a large amount of inductor current i_L and cannot transfer power from the h_1 bridge to the h_2 bridge due to the negative polarity of v_{ab} and v_{cd}. Generally, modes a to c are preferred as they provide optimal converter efficiency.

The inductor current i_L for mode-a at different times t_0, t_1, t_2, t_3 and t_4 can be calculated using Eq. (1), where $t_1 = D_1 T_{sw}/2$, $t_2 = D_2 T_{sw}/2$, $t_3 = D_2 T_{sw}/2$ and $t_4 = D_3 T_{sw}/2$.

Table 1. Phase-shift-ratio range under optimal unified TPS control

Modes	Phase-Shift-Ratio Range
mode-a	$0 \le D_1 \le 1, 0 \le D_1 \le D_2 \le 1, 0 \le D_2 \le D_3 \le 1$
mode-b	$0 \le D_2 \le 1, 0 \le D_2 \le D_1 \le 1, 0 \le D_1 \le D_3 \le 1$
mode-c	$0 \le D_2 \le 1, 0 \le D_2 \le D_3 \le 1, 0 \le D_3 \le D_1 \le 1$
mode-d	$0 \le D_1 \le 1, 0 \le D_1 \le D_2 \le 1, 0 \le 1 + D_1 \le D_3 \le 2$
mode-e	$0 \le D_1 \le 1, 0 \le D_1 \le D_2 \le 1, 1 \le D_3 \le 1 + D_1$
mode-f	$0 \le D_2 \le 1, 0 \le D_2 \le D_1 \le 1, 1 \le D_3 \le 1 + D_1$

$$\left.\begin{aligned} i_L(t_1) &= \frac{nV_2}{L} D_1 \frac{T_{sw}}{2} + i_L(t_0) \\ i_L(t_2) &= \frac{V_1 + nV_2}{L} (D_2 - D_1) \frac{T_{sw}}{2} + i_L(t_1) \\ i_L(t_3) &= \frac{V_1}{L} (D_3 - D_2) \frac{T_{sw}}{2} + i_L(t_2) \\ i_L(t_4) &= \frac{V_1 - nV_2}{L} (1 - D_3) \frac{T_{sw}}{2} + i_L(t_3) \end{aligned}\right\} \quad (1)$$

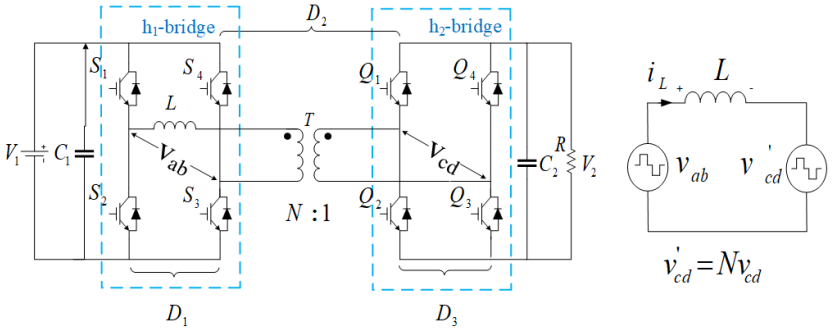

Fig 5. Figure 5 (a). Topology of DAB converter ,(b). Equivalent diagram of DAB converter

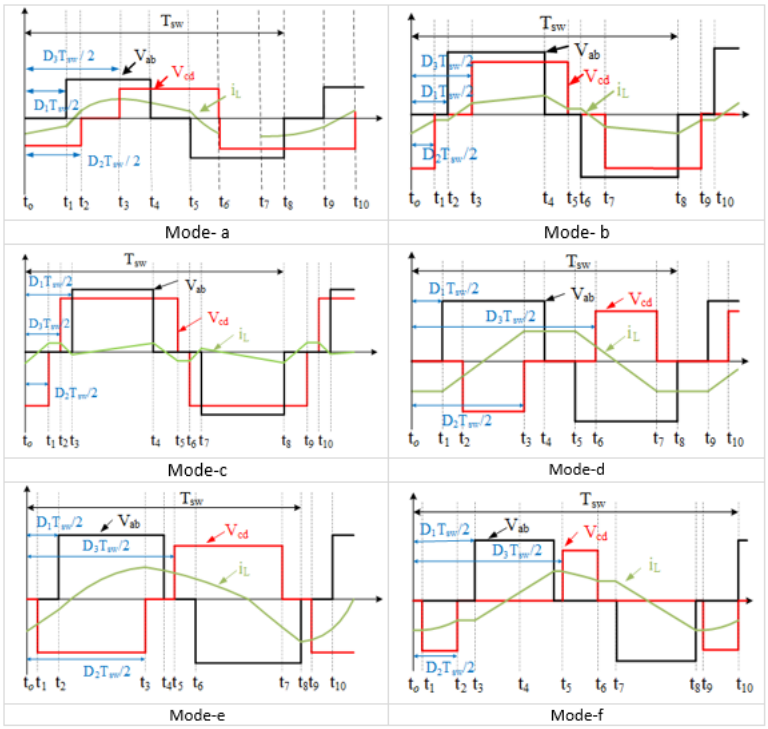

Fig 6. The waveforms of optimal unified TPS controltechnique at different modes and switching periods

Due to its odd symmetry, the inductor current satisfies the condition of $i_L(t_0) = -i_L(t_4)$ during half of the switching period T_{sw} which can be calculated as follows:

$$\left.\begin{aligned} \mathrm{i_L(t_1)} &= \frac{\mathrm{T_{sw}}}{4\mathrm{L}}\left[n\,\mathrm{V_2} + \mathrm{V_1D_1} - \mathrm{V_1} + 2\mathrm{nV_2D_1} - \mathrm{nV_2D_3} - \mathrm{nV_2D_2}\right] \\ \mathrm{i_L(t_2)} &= \frac{\mathrm{T_{sw}}}{4\mathrm{L}}\left[n\,\mathrm{V_2} - \mathrm{V_1D_1} - \mathrm{V_1} + 2\,\mathrm{V_1D_2} - \mathrm{nV_2D_3} + \mathrm{nV_2D_2}\right] \\ \mathrm{i_L(t_3)} &= \frac{\mathrm{T_{sw}}}{4\,\mathrm{L}}\left[n\,\mathrm{V_2} - \mathrm{V_1D_1} - \mathrm{V_1} + 2\,\mathrm{V_1D_3} - \mathrm{nV_2D_3} + \mathrm{nV_2D_2}\right] \\ \mathrm{i_L(t_4)} &= \frac{\mathrm{T_{sw}}}{4\,\mathrm{L}}\left[-\mathrm{nV_2} - \mathrm{V_1D_1} + \mathrm{V_1} + \mathrm{nV_2D_3} + \mathrm{nV_2D_2}\right] \end{aligned}\right\} \tag{2}$$

The power transfer P and inductor current stress S calculation equations for the DAB converter were as follows:

$$\mathrm{P} = \frac{1}{\mathrm{T_{sw}}}\int_0^{\mathrm{T_{sw}}} \mathrm{V_{ab}i_L(t)dt} = \frac{1}{\mathrm{T_{sw}}}\mathrm{V_{ab}}\int_0^{\mathrm{T_{sw}}} \mathrm{i_L(t)dt} \tag{3}$$

$$S = max((i_L(t_0)|,\ (i_L(t_1)|,\ (i_L(t_2)|, \ldots,\ (i_L(t_8)|\}$$

Substituting the values of i_L from Eq. (2) to (3), the power transfer (P) and inductor current stress (S) is derived as:

$$\begin{aligned} P = \frac{v_{ab}}{T_{sw}}dt\int_{t_1}^{t_2}\{i_L(t) - i_L(t_1)\}\,dt + \int_{t_2}^{t_3}\{i_L(t) - i_L(t_2)\}\,dt + \int_{t_3}^{t_4}\Big\{i_L(t) - i_L(t_3) + \int_{t_4}^{t_5}\{i_L(t) - i_L(t_4)\} \\ + \int_{t_5}^{t_6}\{i_L(t) - i_L(t_5)\}\,dt + \int_{t_6}^{t_7}\{i_L(t) - i_L(t_6)\}\,dt + \int_{t_7}^{t_8}\{i_L(t) - i_L(t_7)\}\,dt \end{aligned} \tag{4}$$

$$P = \frac{NV_1V_2T_{sw}\left[D_1D_2 + D_2D_3 - D_1 + D_2 + D_3 - D_1^2 - D_2^2 - D_3^2\right]}{8L} \tag{5}$$

$$S = i_L(t_4) = -i_L(t_8) = \frac{NV_1V_2T_{sw}\left[1 + D_2 + D_3 + \mathrm{k}(1 - D_1)\right]}{8L} \tag{6}$$

In order to simplify the analysis, the power transfer and current stress in per unit system are expressed as:

$$p = \frac{\mathrm{P}}{\mathrm{P_{base}}} = \frac{8\mathrm{LP}}{\mathrm{NV_1\ V_2\ T_{sw}}} = 2\left(D_1D_2 + D_1D_3 - D_1 + D_2 + D_3 - D_1^2 - D_2^2 - D_3^2\right) \tag{7}$$

$$s = \frac{\mathrm{i_{max}}}{\mathrm{i_{base}}} = \frac{8\mathrm{Li_{max}}}{\mathrm{NV_2\ T_{sw}}} = 2\left[1 + D_3 + D_2 + k\left(1 - D_1\right)\right] \tag{8}$$

where p and s are per unit transfer power and current stress, respectively, with p_{base}= rated power and i_{base} = rated current.

Mode-d to mode-f have high inductor current, as a result of reduced converter efficiency. Therefore, these modes cannot be deduced by this analytical method. Only mode-a to mode-c is deduced by this method in which mode-a is discussed above. Similarly, mode-b and mode-c might be determined in the same way. As a result, for the three high-efficiency modes, the power transfer and current stress expressions are as follows:

$$p = \begin{cases} 2\left(D_1D_2 + D_1D_3 - D_1 + D_3 + D_2 - D_1^2 - D_2^2 - D_3^2\right) & \text{mode a} \\ 2\left(-D_1D_2 + D_1D_3 - D_1 + D_2 + D_3 - D_3^2\right) & \text{mode b} \\ 2\left(-D_1D_2 - D_1D_3 - D_1 + D_2 + D_3 + D_1^2\right) & \text{mode c} \end{cases} \tag{9}$$

$$s = \left\{ \begin{array}{c} 2\left[1 + D_2 + D_3 + k\left(1 - D_1\right)\right] \\ 2\left[kD_3 + D_1(1-k)\right] \\ 2\left[2D_2 + D_1(1-k) + D_3(k-2)\right] \\ 2\left[2D_2 + D_1(1-k) - kD_3\right] \end{array} \right\} \text{mode c} \tag{10}$$

The transmission power ranges for mode-a, mode-b, and mode-c are p1 = [0, 1], p2 = [0, 2/3], and p3 = [1/2, 1/2] respectively, as shown in Eq. (9). As can be observed, mode-a has the largest power transfer range, covering the entire operational region, while mode-c can achieve bidirectional power transfer. The current stress for both mode-a and mode-b is the same as derived in Eq. (10). In mode-c, the magnitude of the current stress is governed by both $\mathrm{D_1}$ to $\mathrm{D_3}$ and the transformation ratio (k).

2.2 Optimal Unified TPS Control Strategy

The control strategy comprises two parts: (1) the steady-state part, which aims to minimize current stress, and (2) the dynamic state part, which employs virtual power control to address the DAB converter's dynamic behaviour. To determine the minimal current stress, the Lagrange-multiplier technique (LMM) is commonly utilized[16]. However, the LMM mathematical model has the issue of the power transfer range overlapping in various operating modes[17]. As a result, finding optimal solutions for current stress is challenging due to power transfer and phase shift ratio limitations[18]. The TPS control technique uses a cost function to address the issue of current stress optimization for specific power transfer. Including the cost function in TPS control is intended to overcome the limitations of LMM analysis. The following is the cost function for LMM analysis:

$$\lambda\left(n, g\right) = \frac{\delta S_g}{\delta D_n} \cdot \frac{\delta D_n}{\delta P_g} \tag{11}$$

$D_{n,\,min} \leq \ D_{n,\,otl} \ \leq \ D_{n,\,max}$

Where n denotes the control variable, D_n represents the various phase-shift-ratios, $D_{n,\,min}$ denotes the minimum phase-shift ratio, $D_{n,\,otl}$ denotes the optimal phase-shift ratio, $D_{n,\,max}$ denotes the maximum phase-shift ratio. The operating mode is represented by g, and power transfer and current stress are denoted by P_g and S_g in various modes. The control variables n and g value range between one to three. The parameter λ quantifies the relationship between the fluctuation of the control variable and the corresponding change in cost and gain. To achieve current stress optimization, three cost functions for three distinct modes must be identical, as defined in Eq. (12).

$$\lambda\left(1, g\right) = \lambda\left(2, g\right) = \lambda\left(3, g\right) \tag{12}$$

The above expression is known as cost function optimization (CFO), and through this mode-a is calculated as follows:

$$\begin{cases} \dfrac{-k}{\mathrm{D_3 + D_2 - 2D_1 - 1}} = \dfrac{1}{\mathrm{D_1 - 2D_2 + 1}} \\ \dfrac{-k}{\mathrm{D_3 + D_2 - 2D_1 - 1}} = \dfrac{1}{\mathrm{D_1 - 2D_3 + 1}} \end{cases} \tag{13}$$

After solving the above equation, we get:

$$\begin{cases} \mathrm{D}_{2,\mathrm{ot|}} = \dfrac{k-2}{2(k-1)}\mathrm{D}_{1,\mathrm{ot|}} + \dfrac{1}{2} \\ \mathrm{D}_{3,\mathrm{otl}} = \mathrm{D}_{2,\mathrm{ot|}} \end{cases} \tag{14}$$

where the range of $D_{1,otl}$ is:

$$0 \leq D_{1,otl} \leq \frac{k-1}{k}$$

Similarly, in mode-b, the CFO equation is obtained as follows:

$$\begin{cases} \mathrm{D}_{2,\mathrm{otl}} = (1-\mathrm{D}_{1,\mathrm{otl}})(k-1) \\ \mathrm{D}_{3,\mathrm{otl}} = \mathrm{D}_{2,\mathrm{otl}} \end{cases} \tag{15}$$

Where the range of $D_{1,otl}$ is:

$$0 \leq D_{1,otl} \leq 1$$

For mode-c, the optimized phase-shift relation is difficult to find due to the disturbance in current stress. As the domain boundary is the same for mode-b and mode-c, the optimal result is also equal.

The virtual power component (VPC) is defined below to increase the dynamic performance of the DAB converter:

$$p^* = \frac{\mathrm{V}_{\mathrm{V}}^* \mathrm{V}_2^* \mathrm{i}_2}{\mathrm{V}_2} \tag{16}$$

Where V_2^* is the output reference voltage, PI controller output is denoted by the virtual voltage component (V_v^*), i_2 and V_2 are respectively the measured output current and voltage. The VPC control technique can reduce the sensitivity of the parameter of the converters like total inductance L of the transformer, switching frequency of semiconductor devices, and transformer turn ratio N, and increase the compatibility. The optimal phase-shift ratios ($D_{1,otl}$,$D_{2,otl}$,$D_{3,otl}$) expressed in terms of p^* and voltage conversion ratio (k) is determined by solving Eq. (10), (14), and (15) as follows:

$$\begin{cases} D_{1,\,\mathrm{otl}} = k-1\sqrt{\dfrac{1-p^*}{k^2+2-2k}D_{1,\,\mathrm{otl}}} \\ \mathrm{D}_{2,\,\mathrm{otl}} = \dfrac{1}{2} + \dfrac{k-2}{2}\sqrt{\dfrac{1-\mathrm{p}^*}{k^2+2-2k}} \\ \mathrm{D}_{3,\mathrm{ttl}} = \dfrac{1}{2} + \dfrac{k-2}{2}\sqrt{\dfrac{1-\mathrm{p}^*}{k^2+2-2k}} \end{cases} \tag{17}$$

Similarly, the optimal phase-shift ratios for mode-b and mode-c were equal and as follows:

$$\begin{cases} D_{1,o\,tl} = 1 - \sqrt{\dfrac{p^*}{(k-1)^2}} \\ D_{2,o\,tl} = (k-1) - \sqrt{\dfrac{p^*}{(k-1)^2}} \\ D_{3,o\,tl} = 1 - \sqrt{\dfrac{p^*}{(k-1)^2}} \end{cases} \tag{18}$$

The optimal unified TPC control strategy is presented as a result of the foregoing analysis, as shown in Figure 7 . In this control strategy, output voltage V_2, input voltage V_1, and the output current is extracted using the data acquisition system. Comparing the output voltage and reference voltage with the PI controller results in a virtual voltage component V_v^*. Then the voltage conversion ratio (k) and the virtual power component (p^*) are calculated which decide the operating mode of the DAB converter. With the help of k and p^*, different optimal phase-shift ratios of TPS control are selected from Eq. (17) and (18). Finally, the PWM pulse generator is used to generate the pulse signal for the switches of the DAB converter.

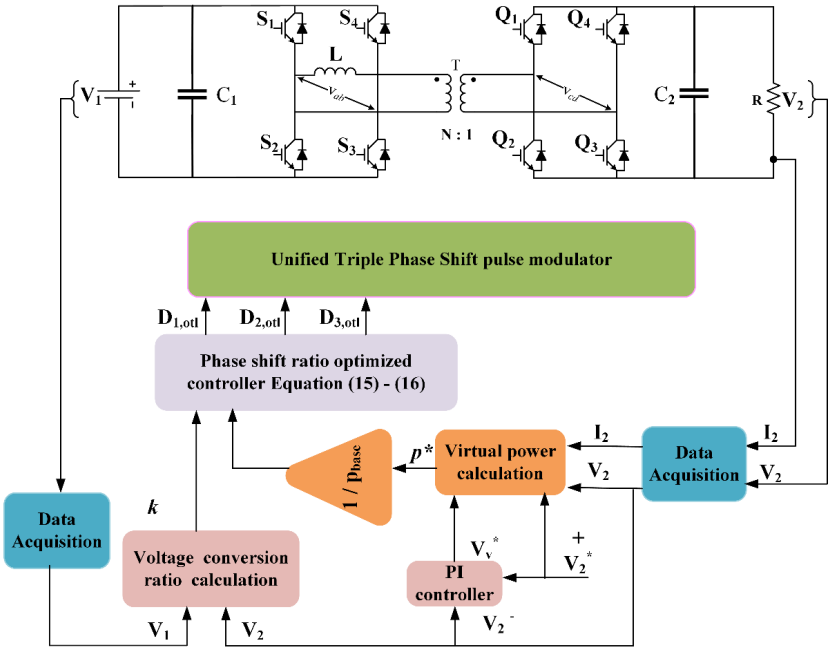

Fig 7. The optimal Unified TPS control strategy

3 Result and Discussion

With the help of the MATLAB Simulink environment, the designed DC-DC DAB converter is simulated. The simulation results are illustrated in the figures below based on appendix. The switching pulses for the DAB converter are shown in Figure 8 , in which $S_1\bar{S}_2$ is the switching pattern for the switch S_1 and the complementary of $S_1\bar{S}_2$ for switch S_2. Similarly, S_3 $\bar{S}_4$, $Q_1\bar{Q}_2$and $Q_3\bar{Q}_4$ are the switching patterns for switches S_3, S_4, Q_1, Q_2, Q_3, and Q_4 respectively. The output voltage, output current, and inductor current with SPS, EPS, and TPS control techniques are shown in Figure 10 . The peak inductor current is 13 A, 10.9 A, and 10 A respectively, viz SPS, EPS, and TPS techniques. Thus, the current stress in the transformer winding is 10 A which is less than the other two control techniques. Figure 9 displays the simulation waveforms of the primary h_1 bridge voltage v_{ab}, the secondary h_2 bridge voltage v_{cd}, and the combination of v_{ab} and v_{cd} where we can see the phase shift between the primary voltage and secondary voltage of HFT, as well as the inductor current i_L .It is observed that v_{cd}lags behind v_{ab}, indicating power flow from the primary to the secondary side, and v_{ab} has a higher amplitude than v_{cd}, suggesting step-down mode operation (k > 1). It is seen that the proposed method exhibits a lower maximum current peak compared to the conventional control technique. This reduction in current stress brings down losses in the converter and power device rating.

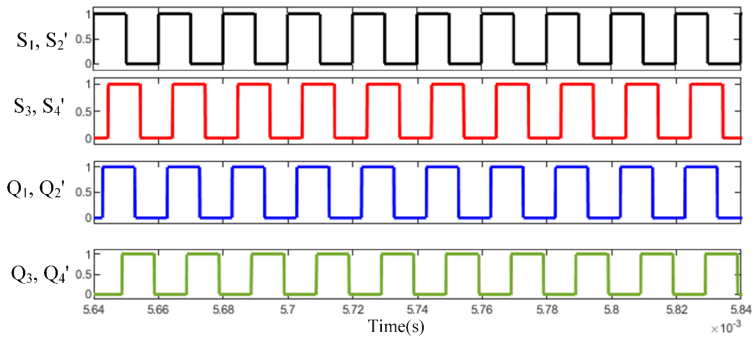

Fig 8. The waveform of the switching pulse of the primary andsecondary h-bridges

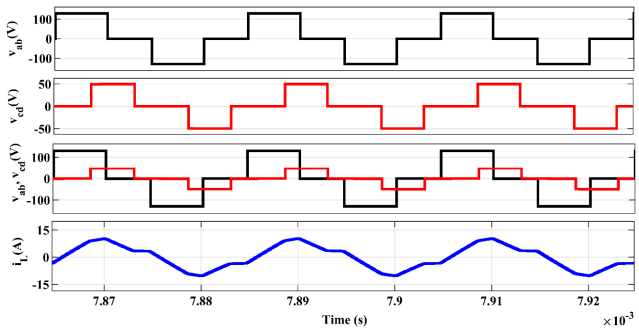

Fig 9. Simulation waveform of the primary bridge voltage , the secondary bridge voltage ,combination of and

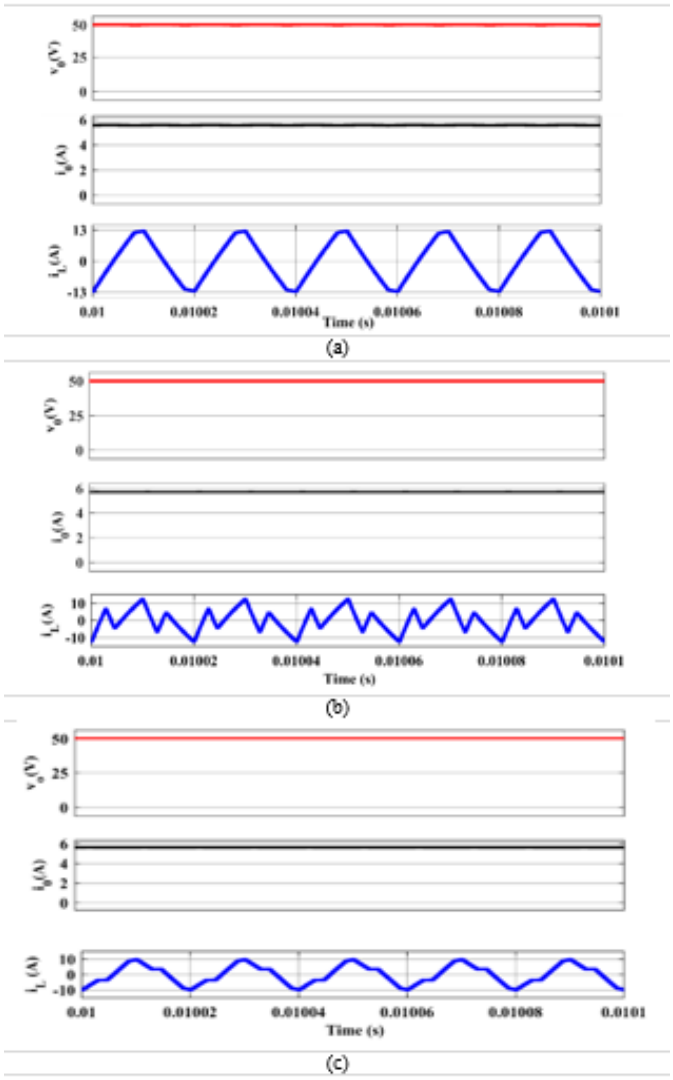

Fig 10. The waveform of output voltage, output and inductorcurrent with (a) SPS (b) EPS (c) TPS control technique

4 Conclusion

The SPS control technique for the DAB converter is commonly employed owing to its simplicity and ease of implementation on hardware but its efficiency decreases when the value of voltage transformation ratio (k) deviates far from unity. Moreover, SPS control does not provide a full power range optimal supply and requires an additional ZVS component that in turn increases the cost. Combining the TPS control technique with the virtual power component minimizes the current stress and therefore improves the efficiency of the DAB converter. This further increases the range of ZVS and minimizes the number of passive components. In this paper, detailed mathematical analysis is carried out and MATLAB Simulink-based simulation results are compared for three control phase shift control techniques viz. SPS, EPS, and TPS, in which 140 V input voltage is converted to 50 V DC output voltage. According to the simulation results, the use of the proposed virtual power control technique results in a 23% and 9% reduction in peak inductor current compared to the conventional SPS and EPS phase shift modulation technique. The proposed optimal TPS control technique shows a stable output voltage and reduced current stress for IGBTs.

Appendix

Input voltage: 140V, output voltage: 50V, input, and output capacitance: 500μF, turn ratio: 52:30, total leakage inductance: 30μH, frequency: 50KHz, load: 5-10 ohm.

References

1) T YH, T JD, Chang CW, Ping J, Yian C, Dahari H. Permanent Magnet Synchronous Generator design optimization for wind energy conversion system: A review. *Energy Reports*. 2022;8:277–282. Available from: https://doi.org/10.1016/j.egyr.2022.10.239.
2) Majout B, Alami HE, Salime H, Laabidine NZ, Mourabit YE, Motahhir S, et al. A Review on Popular Control Applications in Wind Energy Conversion System Based on Permanent Magnet Generator PMSG. *Energies*. 2022;15(17):6238. Available from: https://doi.org/10.3390/en15176238.
3) Takayama Y, Yamada H. Variable DC-Link Voltage Control of Dual Active Bridge Converter in a Standalone Wind Power Generation System for High-Efficiency Battery-Discharging Operation. *Energies*. 2021;14(20):6786. Available from: http://dx.doi.org/10.3390/en14206786.
4) Hannan MA, Ker PJ, Lipu MSH, Choi ZH, Rahman MSA, Muttaqi KM, et al. State of the Art of Solid-State Transformers: Advanced Topologies, Implementation Issues, Recent Progress and Improvements. *IEEE Access*. 2020;8:19113–19132. Available from: https://doi.org/10.1109/ACCESS.2020.2967345.
5) Shadfar H, Pashakolaei MG, Foroud AA. Solid-state transformers: An overview of the concept, topology, and its applications in the smart grid. *International Transactions on Electrical Energy Systems*. 2021;31(9). Available from: https://doi.org/10.1002/2050-7038.12996.
6) Ataullah H, Iqbal T, Khalil IU, Ali U, Blazek V, Prokop L, et al. Analysis of the Dual Active Bridge-Based DC-DC Converter Topologies, High-Frequency Transformer, and Control Techniques. *Energies*. 2022;15(23):8944. Available from: https://doi.org/10.3390/en15238944.
7) Rashwan A, Ali AIM, Senjyu T. Current stress minimization for isolated dual active bridge DC–DC converter. *Scientific Reports*. 2022;12(1). Available from: https://doi.org/10.1038/s41598-022-21359-1.
8) Ansari MR, Palwalia DK. Dual-Active Bridge Converter with Single Phase-Shift Control for Distribution Solid-State Transformer. ICT Analysis and Applications. Lecture Notes in Networks and Systems. vol. 517. Singapore. Springer. 2023. Available from: https://doi.org/10.1007/978-981-19-5224-1_61.
9) Shamshuddin MA, Rojas F, Cardenas R, Pereda J, Diaz M, Kennel R. Solid State Transformers: Concepts, Classification, and Control. *Energies*. 2020;13(9):2319. Available from: https://doi.org/10.3390/en13092319.
10) Jayaswal K, Palwalia DK. Role of reliability assessment in Si-based non-Isolated DC-DC power electronic converters. *Materials Today: Proceedings*. 2022;60:1113–1119. Available from: https://doi.org/10.1016/J.MATPR.2022.02.241.
11) Saeed S, Garcia J, Georgious R. Dual-Active-Bridge Isolated DC–DC Converter With Variable Inductor for Wide Load Range Operation. *IEEE Transactions on Power Electronics*. 2021;36(7):8028–8043. Available from: https://doi.org/10.1109/TPEL.2020.3048928.
12) Huang L, Wang Y. An Improved Phase Shift Control to Reduce Current Stress for Dual Active Bridge DC-DC Converter. *2019 22nd International Conference on Electrical Machines and Systems (ICEMS)*. 2019;p. 1–6. Available from: https://doi.org/10.1109/ICEMS.2019.8921904.
13) Xin L, Haoyu Z, Ya Q, Junkang S. Current stress optimization of dual active bridge converter based on dual phase shift control. *2020 IEEE 9th Joint International Information Technology and Artificial Intelligence Conference (ITAIC)*. 2020;2020:717–741. Available from: https://doi.org/10.1109/ITAIC49862.2020.9339047.
14) Mueller JA, Kimball JW. Modeling Dual Active Bridge Converters in DC Distribution Systems. *IEEE Transactions on Power Electronics*. 2019;34(6):5867–5879. Available from: https://doi.org/10.1109/TPEL.2018.2867434.
15) Hou N, Li YW. Overview and Comparison of Modulation and Control Strategies for a Nonresonant Single-Phase Dual-Active-Bridge DC–DC Converter. *IEEE Transactions on Power Electronics*. 2020;35(3):3148–3172. Available from: https://doi.org/10.1109/TPEL.2019.2927930.
16) Jean-Pierre G, Altin N, Shafei AE, Nasiri A. Overall Efficiency Improvement of a Dual Active Bridge Converter Based on Triple Phase-Shift Control. *Energies*. 2022;15(19):6933. Available from: https://doi.org/10.3390/en15196933.
17) Ríos SJ, Pagano DJ, Lucas KE. Bidirectional Power Sharing for DC Microgrid Enabled by Dual Active Bridge DC-DC Converter. *Energies*. 2021;14(2):404–404. Available from: https://doi.org/10.3390/en14020404.
18) Guzman P, Vazquez N, Liserre M. Indirect Front-End Smart Transformer with Reactive Power Management. *2020 IEEE 9th International Power Electronics and Motion Control Conference (IPEMC2020-ECCE Asia)*. 2020;p. 3482–3489. Available from: https://doi.org/10.1109/IPEMC-ECCEAsia48364.2020.9367850.